N94-14747

The structure of intense vorticity in homogeneous isotropic turbulence

By J. Jiménez[1] , A. A. Wray[2] , P. G. Saffman[3] AND R. S. Rogallo[2]

The structure of the intense vorticity regions is studied in numerically simulated homogeneous, isotropic, equilibrium turbulent flow fields at four different Reynolds numbers in the range $Re_\lambda = 36\text{-}171$. In accordance with previous investigators, this vorticity is found to be organized in coherent, cylindrical or ribbon-like, vortices ("worms"). A statistical study suggests that they are just especially intense features of the background, $O(\omega')$, vorticity. Their radii scale with the Kolmogorov microscale and their lengths with the integral scale of the flow. An interesting observation is that the Reynolds number based on the circulation of the intense vortices, γ/ν, increases monotonically with Re_λ, raising the question of the stability of the structures in the limit of $Re_\lambda \to \infty$. One and two-dimensional statistics of vorticity and strain are presented; they are non-gaussian, and the behavior of their tails depends strongly on the Reynolds number. There is no evidence of convergence to a limiting distribution in our range of Re_λ, even though the energy spectra and the energy dissipation rate show good asymptotic properties in the higher Reynolds number cases. Evidence is presented to show that worms are natural features of the flow and that they do not depend on the particular forcing scheme.

1. Introduction

It is generally agreed that homogeneous isotropic turbulence is approximately described by the Kolmogorov (1941) cascade theory. In particular, the $k^{-5/3}$ energy spectrum and the almost universal scaling of the dissipation range in Kolmogorov variables stand as two of the most successful predictions in fluid mechanics. It has also been known for a long time that this description is incomplete. It was first shown by Batchelor & Townsend (1949) that the statistics of the velocity derivatives are incompatible with an uncorrelated random behavior of the velocity field at scales comparable to the Kolmogorov dissipation limit. This intermittent behavior becomes more pronounced as the Reynolds number increases, and flatness factors ~ 50 have been reported in the atmospheric boundary layer (Van Atta & Antonia, 1980), suggesting that any theory based on uncorrelated gaussian fields might be seriously deficient in the limit $Re \to \infty$. It has to be stressed that, even in these cases, the energy spectrum remains self similar and agrees reasonably well with Kolmogorov's predictions. Energy, and even energy transfer, are large scale or

1 Center for Turbulence Research
2 NASA Ames Research Center
3 California Institute of Technology, Pasadena

inertial range phenomena and do not seem to be strongly affected by intermittency, while the higher moments are associated with rare, intense, small scale events which do not influence the low order statistics.

It is not a priori clear whether this state of affairs will persist for large Re. Moreover, since experiments at much higher Reynolds numbers than those presently available from geophysical flows cannot be expected in the near future, some sort of theoretical understanding of the intermittent small scales is clearly desirable. In this paper we present new data from numerical isotropic homogeneous turbulence at several Reynolds numbers. Even if numerical constraints restrict our experiments to $Re \leq 200$, it may be expected that the exceptional level of detail that can be derived from numerical simulations might help in the theoretical study of the phenomena.

It was discovered recently that strong coherent elongated vortices ("worms") are present among the small scales of many turbulent flows (Siggia, 1981, Kerr, 1985, Hosokawa & Yamamoto, 1990, She *et al.*, 1990, Ruesch & Maxey, 1991, Vincent & Meneguzzi, 1991, Douady *et al.*, 1991), and this discovery generated considerable excitement in the turbulence community. One reason for this interest is that, being strong and therefore presumably decoupled from the influence of other flow components, the behavior of the worms should be relatively easy to understand. Should these vortices be found to form an important part of the turbulence phenomenon, their relative simplicity would give us a tool for the analysis of at least some part of the flow. Failing that, if it could be shown that they are nothing but extreme cases of a more general population of weaker vorticity structures, it might still be true that their study contains some clues as to the behavior of those background vortices, which in turn would constitute an important part of the flow. Even if none of these possibilities turns out to be true, the strong vortices are still relatively simple objects submerged in a turbulent flow, and they may be used as probes for the flow structure.

We will show below that, of these three possibilities, the second seems to be the correct one. In terms of integrated quantities, the strong structures constitute a negligible part of homogeneous isotropic turbulent flows, although they are made conspicuous in flow visualizations by their local high intensities. Moreover, their statistical properties are generally similar to those of the background vorticity, and they seem to be just especially intense realizations of the latter. On the other hand, since they are easy to identify and relatively few in number for any given simulation, their behavior can be studied easily and can be extrapolated to a description of the behavior of the background.

2. The numerical experiments

Our observations are made on direct numerical simulations of isotropic homogeneous turbulence in triply periodic boxes at four different Reynolds numbers ranging from $Re_\lambda = 36$ to 170. It is surprising that we are able to find similarity laws spanning the whole range of Reynolds numbers, and that even the lowest Re_λ flow seems to be essentially turbulent. This gives us some confidence that our observations may represent asymptotic trends for high Reynolds number turbulence.

Line	Re_λ	N	L	L/λ	L/η	$\epsilon L/u'^3$	$\omega'T$	t/T	$-S_k$
Chaindot	35.8	64	2.02	2.59	31	1.08	10.0	12.8	0.496
Dotted	62.8	128	1.87	3.54	56	0.83	13.0	5.3	0.503
Dashed	94.5	256	1.31	4.21	80	0.66	16.2	7.6	0.518
Solid	171.5	256	1.62	7.50	193	0.65	29.0	5.9	0.500

TABLE 1. Numerical and flow parameters for the four basic cases analyzed in this paper. t/T is the total run time in eddy turnover units, and S_k is the skewness coefficient. Line types are used consistently in later figures.

The numerical method is fully spectral, using primitive variables u, p, with dealiasing achieved by a spherical mask and phase shifting (Canuto et al., 1987). The resolution N, given in Table 1, reflects the number of real Fourier modes in each direction before dealiasing. The time stepping procedure is a second order Runge-Kutta for the nonlinear terms and an analytic integrating factor for the viscous ones. The time step is automatically controlled to satisfy the numerical stability condition. Unless stated otherwise, all experiments are forced to achieve a statistically stationary steady state. Forcing is achieved by introducing a negative viscosity coefficient for all the modes with wave numbers $k = |\mathbf{k}| \leq 2$. The Fourier expansion functions are $\exp(ik_j x_j)$, $k_j = 0, 1, \ldots, K = N/2$, so that the length of the box side is always 2π. The magnitude of the negative viscosity is adjusted every few time steps so as to keep constant the product $K\eta$, where $\eta = (\nu^3/\epsilon)^{1/4}$ is the Kolmogorov scale. The instantaneous energy dissipation rate, ϵ, is computed in terms of the three dimensional energy spectrum $E(k)$, as

$$\epsilon = \nu\omega'^2 = 2\nu \int_0^\infty k^2 E(k)\,dk.$$

Other scales used in this paper are the r.m.s. velocity, defined by

$$u'^2 = \frac{2}{3} \int_0^\infty E(k)\,dk,$$

the integral scale,

$$L = \frac{\pi}{2u'^2} \int_0^\infty k^{-1}E(k)\,dk,$$

and the Taylor microscale, defined by $\lambda^2 = 15\nu u'^2/\epsilon$. The microscale Reynolds number is defined as $Re_\lambda = u'\lambda/\nu$, and the large eddy turnover time as $T = L/u'$ (Batchelor, 1953).

Table 1 summarizes the characteristics of the different runs. Each of them was continued sufficiently long for the instantaneous spectra and other integral characteristics to become statistically steady. This typically took a few large eddy times,
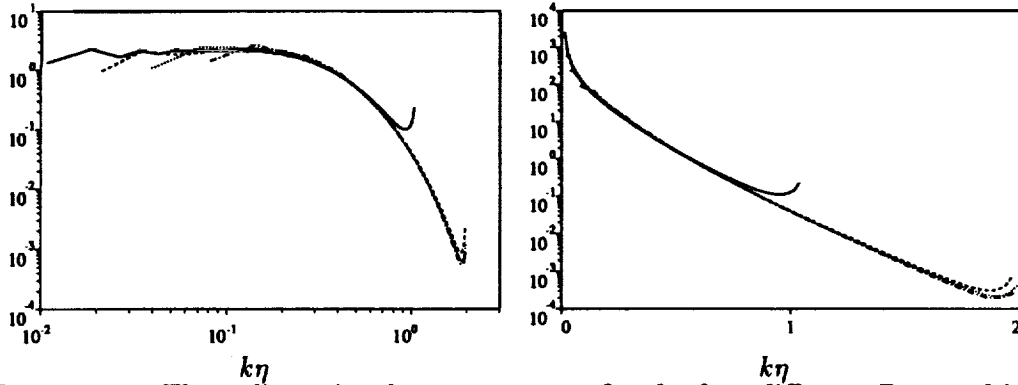
FIGURE 1.   Three dimensional energy spectra for the four different Re_λ used in this paper. Left: $\epsilon^{-2/3}k^{5/3}E(k)$, to enhance inertial range. Right: $\epsilon^{-2/3}\eta^{-5/3}E(k)$, to display the dissipation range. For symbols see table 1.
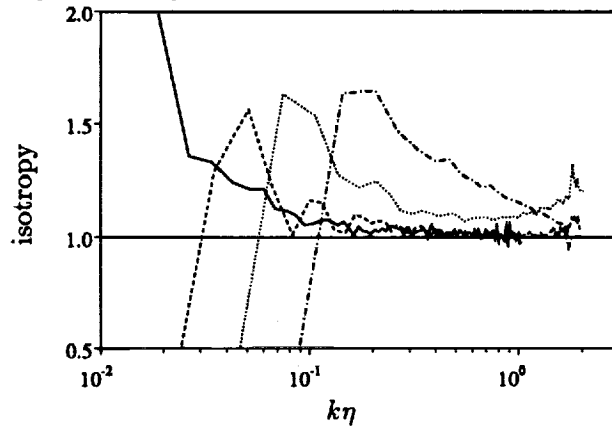

FIGURE 2.   Isotropy coefficient for different Reynolds numbers, defined in eq. (1) in text. Symbols as in table 1.

which may not be long enough to guarantee absolute statistical steadiness for the large scales, but which should be enough for the small scales to reach equilibrium. The quantities in table 1 and the spectra in the following pages are averages over whole flow fields and over periods of time that vary between 0.25 and 6 large eddy turnover times. The shorter averaging times correspond to the highest Reynolds numbers. The histograms presented later in the paper are spatial statistics, further averaged over 3 to 5 different moments in time. The variation between the averaged spectra and their instantaneous values was smaller that 1%, but larger deviations were observed in the extreme tails of the histograms.

Note that the dimensionless energy dissipation $\epsilon L/u'^3$ decays slowly with Re_λ but stabilizes around 0.65 in the last two cases. This is consistent with the behavior observed by Sreenivasan (1984) in a compilation of data from grid turbulence, in which the dissipation stabilizes above approximately $Re_\lambda > 60$. His asymptotic value of the dissipation, $\epsilon L/u'^3 \approx 1$, is different from ours, but this is not too surprising since

the integral scale is dominated by the large eddies, which are presumably different in the two cases.

The statistics of the small scale intense regions are sensitive to the numerical resolution. After some experimentation, it was found that $K\eta = 1$ was the absolute minimum needed for convergence of the velocity gradients histograms, and that $K\eta = 2$ was very desirable. We tried to maintain this latter resolution uniformly, but it was not possible to do so for the highest Reynolds number case during the time limits of the summer school. In the experiments presented here, this case is only resolved to $K\eta = 1$.

Three dimensional, shell averaged, energy spectra for the three cases are presented in figure 1. The two cases with the highest Re_λ show a short "inertial" range with a power decay close to $k^{-5/3}$. No such interval is present at the lowest Re_λ, but the collapse of the dissipation range is satisfactory. Figure 2 displays an isotropy coefficient, defined by

$$\frac{E_{11}(k_1) - k_1 \partial E_{11}(k_1)/\partial k_1}{2E_{22}(k_1)}, \tag{1}$$

where E_{11} and E_{22} are the longitudinal and transverse one dimensional spectra. This quantity should become equal to 1.0 for an isotropic field (Batchelor, 1953), and it does so approximately for the small scales in the two high Re_λ cases, suggesting that the they have attained equilibrium. The two cases with lower Reynolds numbers do not satisfy isotropy, and this is true as much for individual realizations as for averages over fairly long times, although the direction of the deviation is different for different realizations. This lack of isotropy is probably due to the relatively low number of structures contained in such low Reynolds number flows.

In summary, the flows used in this paper seem to be typical of experimental approximations to homogeneous isotropic turbulence. It is particularly important to note that the two highest Reynolds numbers display a short $k^{-5/3}$ inertial range and appear to have reached the asymptotic regime in which energy dissipation becomes independent of the Reynolds number.

3. Worms

Implicit in the Kolmogorov (1941) model for the turbulent cascade is the idea that the small scales of turbulence are fully controlled by the viscosity ν and by the energy dissipation rate $\epsilon = \nu\omega'^2$. This and the dimensional arguments of the original theory imply that the velocity gradients should reach some asymptotic statistical distribution as $Re \to \infty$, whose single scale should be ω'. Evidence that this is not so has accumulated over the years, starting with the measurements of higher statistical moments mentioned earlier and more recently in the form of increasingly non-gaussian histograms obtained from numerical experiments at increasing Reynolds number (Siggia, 1981, She *et al.*, 1990, Vincent and Meneguzzi, 1991, Ruetsch & Maxey, 1991). We will concentrate here on the statistics of the quantities appearing directly in the vorticity equation,

$$\frac{d\,|\omega|^2/2}{dt} = \omega_i S_{ij}\omega_j + \nu\omega_i\nabla^2\omega_i, \tag{2}$$
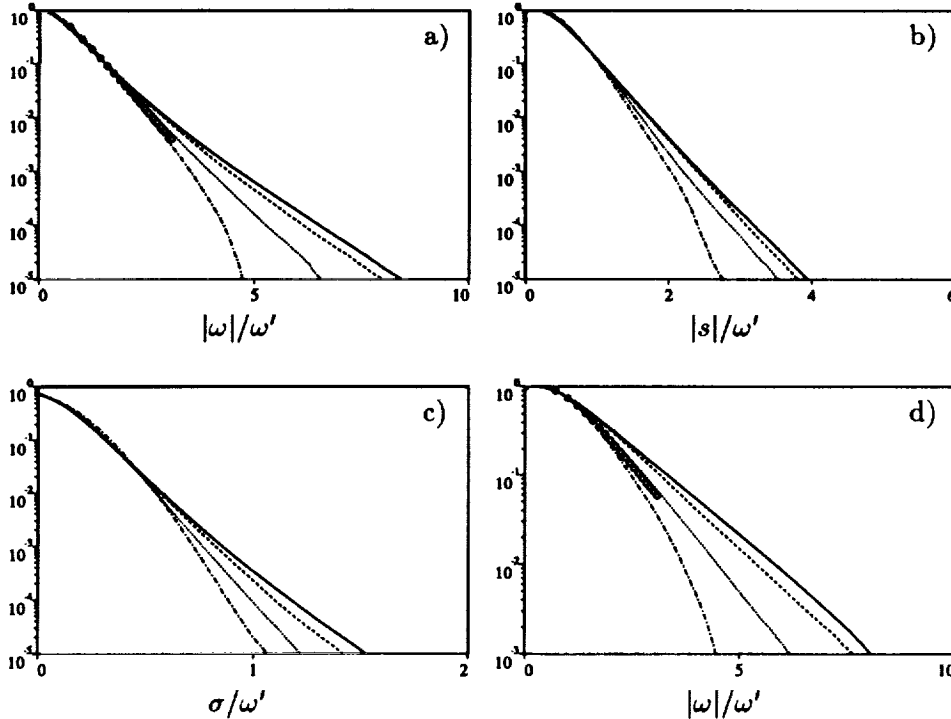
FIGURE 3.   One dimensional histograms of the volume fraction occupied by points above a certain threshold. (a) Vorticity, (b) Strain, (c) Stretching. (d) Fraction of total enstrophy associated with points above a given vorticity magnitude. Lines as in table 1. Open circles are from (Ruetsch & Maxey, 1991) at $Re_\lambda = 62$.

where $|\omega| = (\omega_i\omega_i)^{1/2}$ is the vorticity magnitude, and $S_{ij} = (\partial u_i/\partial x_j + \partial u_j/\partial x_i)/2$ is the rate of strain tensor. In particular, we will be interested in the statistics for $|\omega|$, $|s| = (S_{ij}S_{ij})^{1/2}$, and

$$\sigma = \frac{\omega_i S_{ij}\omega_j}{|\omega|^2}.$$

The square of the total rate of strain, $|s|$, is proportional to the local dissipation, but it does not appear explicitly in equation (2). It is probably more a consequence of the events that lead to turbulence than their cause. The quantity σ is the part of the strain which is aligned to the local vorticity, and it is the one doing the stretching of the vortex lines in equation (2). Its mean value is related to the skewness of the velocity derivatives.

One dimensional histograms for the volume fraction occupied by values of these three variables above a given threshold are given in figure 3. They are all far from gaussian, except perhaps for the lowest Reynolds number, and show few signs of converging to a limit distribution for large Re_λ. Note, however, that the variable tails involve only relatively small fractions of the total volume. The figure also contains a histogram for the fraction of the total enstrophy contributed by points with a vorticity magnitude above a given threshold. Even if the decay of this
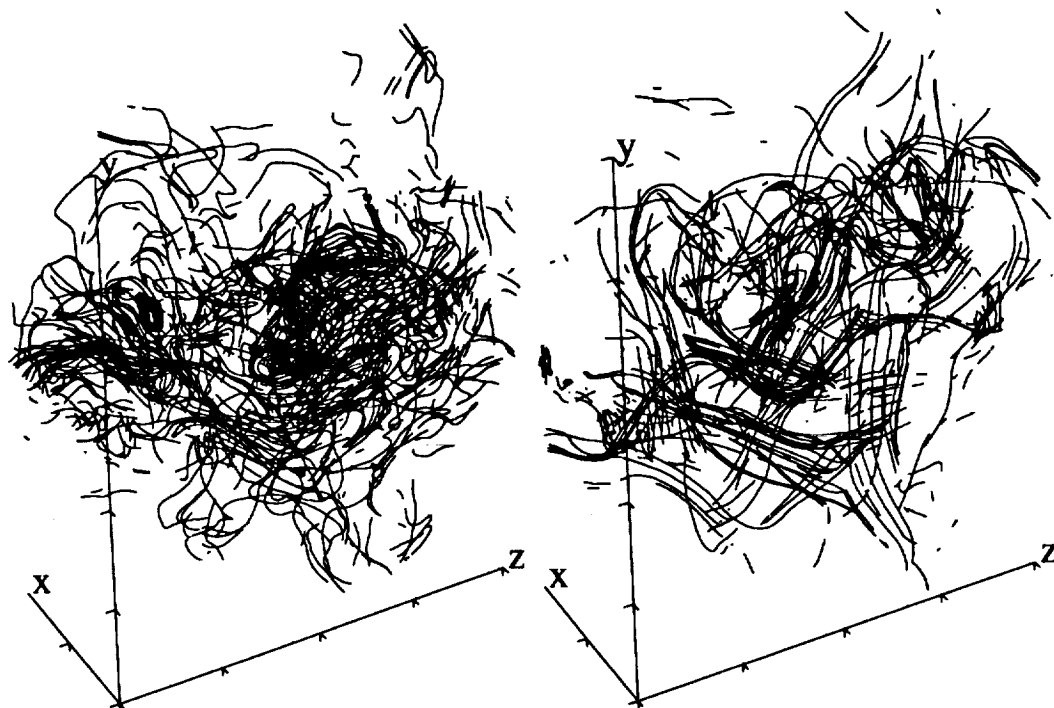
FIGURE 4. Vortex lines for homogeneous isotropic turbulence, $Re_\lambda = 209$. Length of z-axis $\approx 100\eta$. Left: Only $0.2\omega' < |\omega| < \omega'$; Right: Only $|\omega| > \omega'$; Vortex lines are the same in both sets.

histogram is slower than that of the volume fraction, most of the enstrophy is still contained in a relatively "weak" background where $|\omega| \approx O(\omega')$. In fact, for the Reynolds numbers of our simulations, the contribution of the intense tails to the integrated value of any of the low order statistics of the flow is only a few percent, although they would clearly dominate sufficiently high order moments. Similar results were obtained by Ruetsch and Maxey (1991) at $Re_\lambda \approx 60$ (see fig. 3).

The conclusion from these histograms is that most of the volume in the flow is occupied by relatively "weak" vorticity with strong vortices filling only a small fraction of the space. The structures of the weak and strong vorticities are also very different. Figure 4 shows a collection of vortex lines passing through randomly chosen points on the middle plane of a subset of a high Re_λ simulation and continuing until they leave the cube. The vortex lines are exactly the same in both cases, but in the left hand side of the figure they are only displayed where $0.2\omega' \leq |\omega| \leq \omega'$, while in the right hand side they are displayed where $|\omega| \geq \omega'$. While there is little apparent structure in the low intensity component of the flow, the strong vorticity tends to be organized in tubes or ribbons, which are the "worms" reported in previous experiments. It is remarkable that this seems to be true even at a threshold, ω', which is much lower that the one used in most previous reports, and which still contains most of the total enstrophy.

For the rest of the paper, we will arbitrarily define *weak* vorticity as that having

FIGURE 5.   Intense vorticity isosurfaces, $|\omega|/\omega' \geq 2.5$, at two different Reynolds numbers. Resolution is similar in both subsets, with the length of each axis $\approx 100\eta$. Left: $Re_\lambda = 63$, integral scale $L = 56\eta$. Right: $Re_\lambda = 95$, $L = 80\eta$. Thresholds are chosen so that worms contain about 1% of total flow volume.

$|\omega| < \omega'$, *intense* vorticity, or *worms*, as that above a threshold covering 1% of the total volume, and *background* vorticity as that above ω' but weaker than the intense threshold. This definition of worms results in pictures roughly comparable to those of previous experimenters and is about as low as the threshold can be taken before the visual complication becomes overwhelming. Figure 4 shows that the organization in coherent structures is still present at the background level. At the Reynolds number of the figure, the vorticity above ω' fills 25% of the volume and accounts for 80% of the total enstrophy, while intense vorticity fills 1% of the volume and accounts for 15% of the enstrophy.

The length of the horizontal (z) axis in figure 4 is one eighth of that of the whole cube and one half of the integral scale of the flow. Some ribbons are seen to span the whole subset, although not with uniform intensity, and they may appear disconnected in plots of the high enstrophy worms. Long intense worms, comparable to the integral scale, are found occasionally.

The shape of the regions of highest vorticity (1%) is displayed in figure 5 at two different Reynolds numbers. In agreement with previous reports, they are shown to be either cylindrical vortices or ribbons of various widths. Although no real statistical analysis was made, the impression from different fields is that sheets and ribbons are predominant at low Reynolds numbers, while cylindrical vortices dominate at high Re_λ. This is apparent in figure 5 and is consistent with the idea that the worms are the result of stretching by strains which are generally not axisymmetric.

If a generic strain is applied to a weak vorticity blob, the vorticity component along the most extensional eigenvector is amplified most, but the other two principal strains remain active and try to stretch or compress the vortex unequally along the two equatorial axes. As the axial vorticity becomes stronger, it dominates the local flow and its rotation tends to make the vortex axisymmetric. The result is a vortex of elliptical cross section whose eccentricity becomes smaller as the ratio of the axial vorticity to the driving strain becomes larger. It will be shown later that the strain is generally $O(\omega')$, while it is clear from figure 3 that vortices in higher Reynolds number flows attain larger vorticities. This, together with the previous argument, explains their more circular cross sections.

The spatial distribution of the worms is not uniform, although this is difficult to see in graphical representations of large subsets. Figure 6 displays a thin slab across a complete flow field. The worms are seen to lie on the borders of large scale velocity eddies, the energy containing scales, which are themselves relatively free from vorticity. This is even clearer in figure 7, which represents the mid-plane of the slab in the previous one. The light colored regions in this figure mark the background vorticity, $|\omega| > \omega'$. The darker regions are the worms, which are seen to be embedded in the background of which they constitute the local maxima. The large eddies themselves are mostly free even from background vorticity.

4. Truncated fields

Even if the results in the previous section suggest that, at least at these Reynolds numbers, the worms contribute relatively little to the turbulent statistics, it is conceivable that they may be important indirectly in some other respect. There is also the possibility that the worms themselves may be spurious effects of the forcing method and that they would not be present in "natural", decaying turbulence.

To clarify these points, we have carried out a series of experiments in which the worms are artificially removed from a flow and in which both the properties of the truncated field and those of the isolated worms are studied independently. Consider a flow field given by a velocity $\mathbf{u}(\mathbf{x})$ and a vorticity $\omega = \text{rot } \mathbf{u}$. We wish to generate a new field $\mathbf{u}_>$, associated just with the worms, by eliminating the vorticity at points where its magnitude is smaller than a given threshold, $|\omega| \leq \Omega$. This field cannot be constructed by just zeroing the vorticity of the original flow at the desired points. The resulting vortex lines would not be closed, and no velocity could be constructed. Consider the naively truncated field

$$\omega_o = \omega \quad \text{if} \quad |\omega| > \Omega, \qquad \omega_o = 0 \quad \text{otherwise.} \tag{3}$$

This field is generally not solenoidal, $\text{div } \omega_o \neq 0$. We define the worms as the field $\omega_> = \omega_o + \Delta$ such that $\text{div } \omega_> = 0$ and such that the extra enstrophy $\int |\Delta|^2 \, d\mathbf{x}$ is as small as possible. Note that vorticity of this field is not strictly zero outside the worms, but that the construction guarantees that the undesired residual is a minimum. It follows from straightforward variational analysis that $\Delta = -\nabla \lambda$, where the scalar λ satisfies $\nabla^2 \lambda = \text{div } \omega_o$.
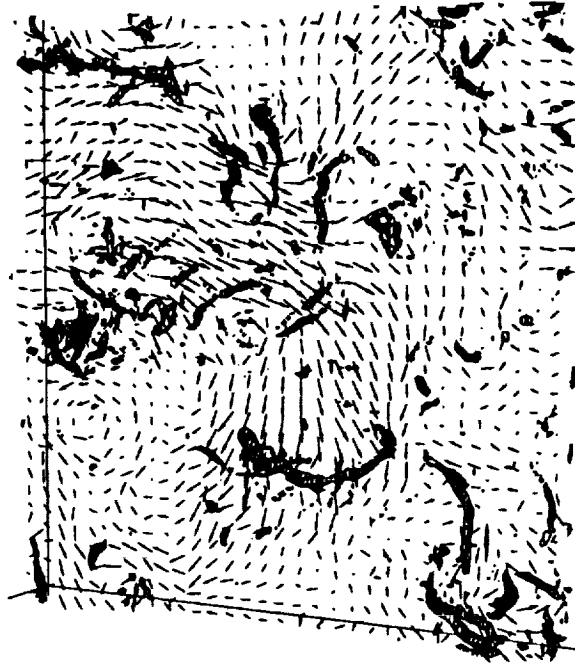
FIGURE 6. Intense vorticity regions $|\omega| > 2.7\omega'$, and velocity field, $Re_\lambda = 209$. Size of the display domain, $(800^2 \times 50)\eta$, periodic in the two long directions. Velocity vectors correspond to points in the mid plane.
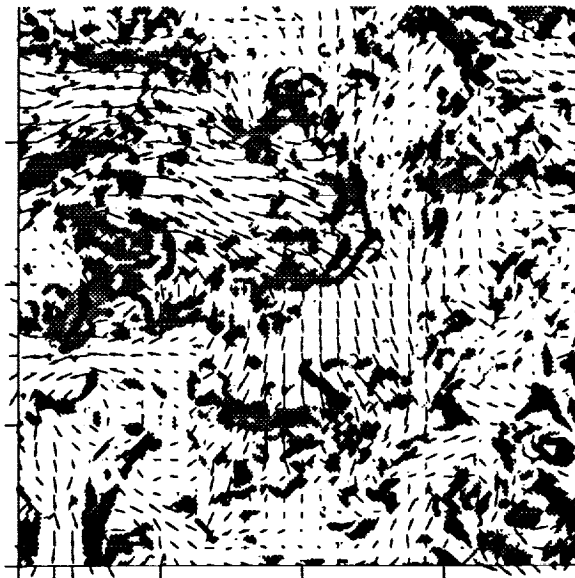

FIGURE 7. Background vorticity $|\omega| > \omega'$ (light gray), at center plane in figure 6, in relation to darker intense regions, $|\omega| > 2.7\omega'$. Vectors are velocity.
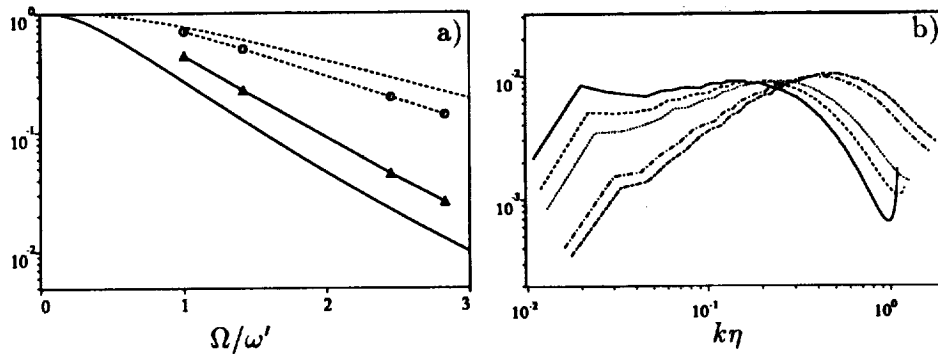
FIGURE 8. Effect of the truncation threshold on the worm fields truncated to $|\omega| > \Omega$ as described in text. (a) Simple solid line: volume fraction above vorticity threshold in original field. Dashed: enstrophy above threshold. Dashed with circles: Enstrophy of truncated field, as fraction of original. Solid with triangles: Kinetic energy of truncated field. (b) Enstrophy spectra. Threshold in order of decreasing enstrophy at low wave numbers: Ω/ω': 0., 1., 1.41, 2.45, 2.83. $Re_\lambda = 209$.

Note that the new field is nothing but the solenoidal projection of ω_o and that a velocity can be computed from it.

The effect of this truncation is shown in figure 8a, which displays both the enstrophy and kinetic energy of the truncated worm fields as a function of the threshold as well as the volume and enstrophy associated to regions of the original field whose vorticity is above that threshold. It is seen that the effect of the projection is to decrease only slightly the enstrophy contained in the worms. A visual check of the corresponding enstrophy isosurfaces confirms that the intense regions in the truncated field correspond to those of the original one but that the vorticity in the background has been mostly eliminated. The energy of the truncated flow is always small, roughly proportional to the volume occupied by the worms themselves. There seems to be no appreciable local enhancement of the kinetic energy because of the presence of the worms. This is confirmed by inspection of the velocity fields in figures 6 and 7.

Similar experiments on the truncated background fields, resulting from the removal of the vorticity above a given threshold, reveal a complementary effect. The effect of removing the worms is small, both on the enstrophy and on the energy, and it only becomes appreciable when the truncation threshold is made comparable to ω'.

In addition, no particular part of the energy spectrum seems to be especially associated with the worms. Figure 8b displays enstrophy spectra, $2k^2E(k)$, for the high vorticity component at different truncation thresholds, each of them normalized by its own Kolmogorov scaling. The spectrum of the original field is consistent with an inertial range, $E(k) \sim k^{-5/3}$, while that of the high intensity worms is close to $E(k) \sim k^{-1}$, but the effect is gradual, proportional to the removal of the total kinetic energy. The latter spectrum was shown by Townsend (1951) to be that of a random array of vortex tubes of uniform radii and is, therefore, consistent with the
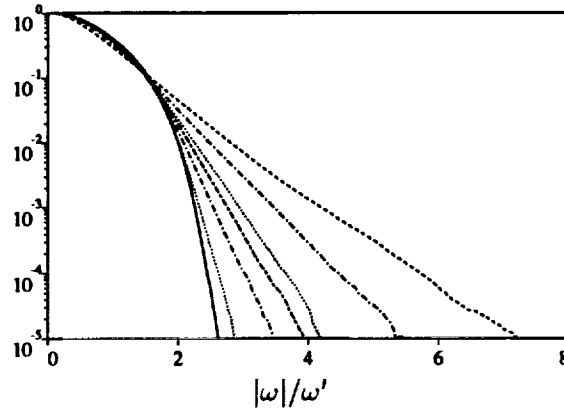
FIGURE 9.   Time evolution of the histograms of volume fraction above a given vorticity threshold, during decay of a flow field initially truncated to $|\omega| < 1.5\omega'$. $Re_\lambda = 96$. Decay time, left to right: $u't/L = 0$, 0.019, 0.037, 0.056, 0.073, 0.158. All normalizations refer to the initial field before truncation.

general structure of the worms.

Since the integral of the dissipation is proportional to that of the enstrophy, the effect of removing the worms, which contain only a small percentage of the latter, is not expected to have a large effect on the decay of the kinetic energy of a turbulent field. This was tested directly by comparing the evolution of the decay of identical initial conditions with and without the worms removed. An equilibrium field was generated ($Re_\lambda = 96$), and the forcing was removed to initiate a decay. The same initial conditions were truncated to $|\omega| < 2.5\omega'$ and left to decay. The behavior of the energy in both cases was almost identical when normalized with the initial enstrophy of each field. The enstrophy of the truncated field decayed initially faster but, after a short transient during which it decayed by about 7%, it also behaved similarly to that of the equilibrium initial condition. The difference in the total enstrophy of the initial fields at this truncation level was 20%.

A more severe truncation was applied to check whether the presence of the worms could be somehow associated with the forcing scheme. The same flow field as in the previous experiment was truncated to $|\omega| < 1.5\omega'$ and left to decay. Figure 9 shows the time evolution of the volume fraction histograms. It is clear that, after a short time, the worms reappear even in the absence of forcing. This was checked directly by visualization.

It follows from these experiments that the worms are a natural product of the evolution of turbulent flows, both forced and decaying, and that their importance in the dynamics of turbulence is only proportional to the magnitude of their integrated quantities with respect to those of the whole flow. They do not seem to play any special role besides that which corresponds to the energy and enstrophy that they contain. At the Reynolds numbers of our experiments, both are small fractions of the total.

An interesting observation is that the skewness coefficient of the truncated worm

fields, those formed only by the high intensity regions, was always negative and roughly of the same order as that of the full turbulent field ($S_k = -.5$ to -1.0). The high intensity regions are still straining each other, and they would be capable of generating new enstrophy, although the relatively low kinetic energy that they contain means that the Reynolds number of the truncated flow is low and that the viscous diffusion would dominate before any appreciable evolution is possible.

5. The dynamics of worm formation

Even if the worms do not seem to have a special function in the overall dynamics of turbulent flows, the process by which they are formed is interesting in itself. Moreover, since they appear to be part of the general $O(\omega')$ background vorticity, we may look at them as particular cases of the evolution of that component, which is responsible for most of the turbulent dissipation. Finally, since they do not scale correctly in Kolmogorov variables (i.e. the histograms do not scale with ω'), their generation mechanisms might point to some deficiency in the standard cascade theory, especially as $Re_\lambda \to \infty$.

Qualitatively, it is clear that strong vortex regions have to be formed by straining of weaker vorticity. No other mechanism is available, away from no-slip walls, for the production of enstrophy. Strain itself is generated by the vorticity, and the process may become nonlinear. It has been realized for some time that nonlinear self interaction of vorticity can, in principle, lead to a singularity of the inviscid equations in finite time and that it may therefore be invoked to explain the generation of vorticity of almost any magnitude.

Some orders of magnitude might be relevant at this point. If we apply a strain α to a viscous fluid, the smallest flow features that we may expect to generate are of the order of the Burgers' radius, $\delta = (\nu/\alpha)^{1/2}$. There are two "natural" straining scales in turbulence: the strain generated by the large eddies, $1/T = u'/L$, and the inverse of the Kolmogorov time scale, which is equal to the r.m.s. vorticity $\omega' = (\epsilon/\nu)^{1/2}$. The Burgers' radius for the former is the Taylor microscale λ, while that for the latter is the Kolmogorov η. Moreover, if we think of a cylindrical equilibrium Burgers' vortex generated by a strain α, its peak vorticity would be $\omega_{max} \sim Re_\gamma \alpha$, where $Re_\gamma = \gamma/\nu$ is a vortex Reynolds number based on its total circulation. If we assume, e.g. on stability grounds, that Re_γ cannot be larger than a given limit independent of the applied strain, the peak vorticity should never be more that a fixed multiple of the strain.

We have evidence in the histograms in figure 3 that some component of the turbulent flow contains peak vorticities that increase with Reynolds number faster that ω'. From the previous discussion, this implies either that there exist stretching motions which are stronger than ω' or that there exist vortices whose Re_γ grows larger as Re_λ increases. The first possibility implies that we should find structures whose transverse scale is smaller than η and that this discrepancy should increase with increasing Re_λ. This contradicts the relatively good collapse of the energy spectra in the dissipation range, expressed in Kolmogorov variables, although some weak effect can not be ruled out from the experiments. The second possibility raises

Re_λ	ℓ/L	R/η	$Re_\gamma/Re_\lambda^{1/2}$	N_w
35.8	3.16	4.22	21.1	26
62.8	2.60	4.16	17.0	32
94.5	3.15	4.16	18.1	14
171.5	2.88	4.61	21.1	15

TABLE 2. Average worm parameters as identified by the tracking algorithm defined in the text. N_w is the number of worms in each sample, ℓ their average length, and R their radius.
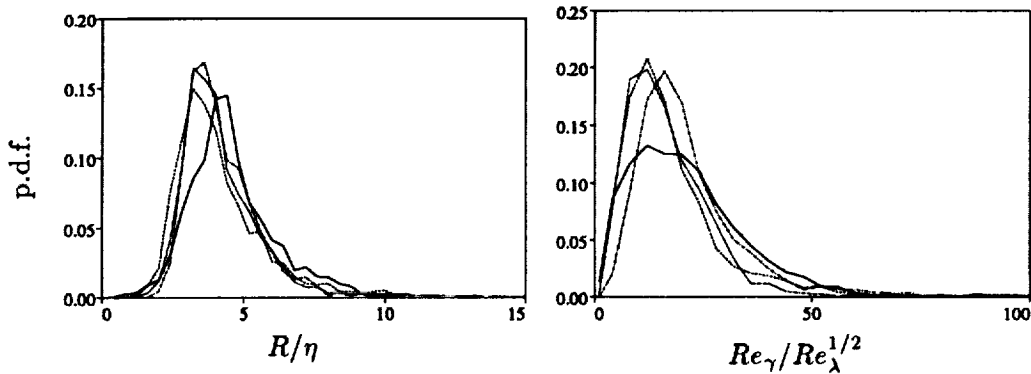

FIGURE 10. Probability density functions for worm radii and circulations at four different Reynolds numbers. Symbols as in table 1. Normalization has been chosen so as to optimize collapse.

the question of how such high Reynolds number vortices remain stable long enough to form.

To answer this question, we undertook a statistical investigation of the dimensions and circulation of the intense vorticity structures. Most of the previous investigators who have treated this subject give their radii as a few Kolmogorov scales and their lengths as being of the order of the integral scale. A survey including some new measurements of radii and intensity is contained in Jiménez (1991). It was concluded that, for the available flow fields, the average radius was approximately 3-5η, and $Re_\gamma \approx$ 150-400. It was noted, however, that most of the data had $Re_\lambda \approx$ 100 and that no reliable scaling trend could be deduced. We believe that the present investigation is the first one in which enough data sets with uniform resolution and overall quality have been collected over a wide enough range of Reynolds numbers to allow for some scaling information.

An automatic tracking algorithm, described in detail in the appendix, was implemented and applied uniformly to all the data fields. Briefly, a point in the worm axis is identified as a vorticity maximum, and the axis is followed until either its
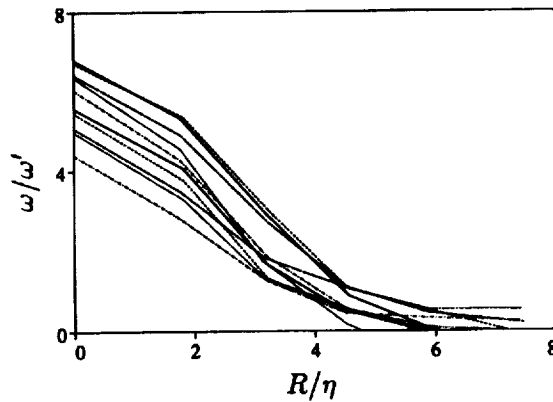
FIGURE 11. Radial vorticity distribution for different cross sections along a typical worm. $Re_\lambda = 62.8$.

peak vorticity falls below ω' or until the worm closes into itself or intersects a previously known one. At each point in the axis, the vorticity in a normal plane is averaged azimuthally, and the resulting radial distribution is fitted to a gaussian. The local radius of the worm is defined as the $1/e$ radius of the gaussian, and the circulation as that of the fitted distribution. It was, unfortunately, impractical to continue this process until no more worms could be found, and the samples used here represent what could be achieved in a fixed amount of computer time (3 hours). A rough estimate of the total volume of the worms in the sample compared to the volume occupied by vorticity above ω' suggests that the sample contains most of the worms in the lowest Reynolds number case, but only about 1% of them in the highest one. Average values of worm length, radius, and circulation are given in table 2. A comparison with the range of scales in table 1 is enough to show that the normalizations chosen here are fairly robust, at least in this range of Re_λ, and that other choices would lead to significant trends. In particular, the worms radii scale with η and their lengths with the integral scale L, and their circulation increases as $Re_\lambda^{1/2}$.

The trends of the radii and circulations are consistent with those observed in Jiménez (1991) for the intense longitudinal vortices in the wall region of a turbulent channel. It was shown there on the basis of rather limited data that the radii of the vortices scale well in wall units, within a range of Reynolds numbers $Re_\tau = 100$-200. The circulations, however, do not remain constant, and increase by almost a factor of two in the same range. Since wall units are the near wall equivalent of Kolmogorov scaling, those trends are equivalent to the ones observed here. In the same spirit, the recently established tendency of turbulent fluctuations to increase with Re_τ beyond their dependence in wall units (Wei & Willmarth, 1989) can be considered as related to the failure of Kolmogorov scaling in figure 3.

Actual probability density distributions of radii and circulations are given in figure 10 and a sample of azimuthally averaged vorticity profiles across a typical worm is given in figure 11, showing that the gaussian model is at least reasonable. This
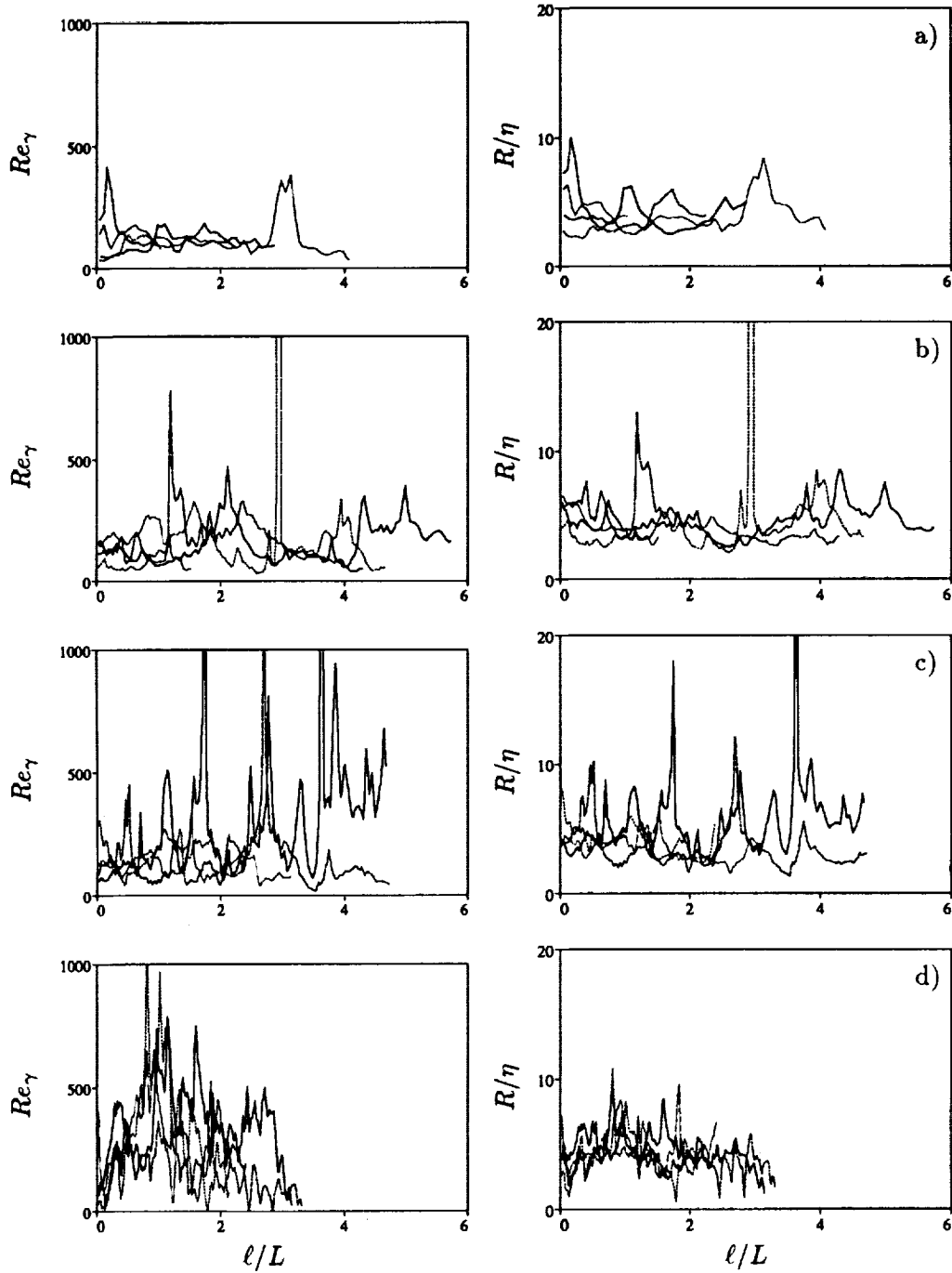
FIGURE 12.   Distribution of normalized radii and circulations along worm axes as function of arc length ℓ.   Each figure contains four worms chosen at random.   (a) $Re_\lambda = 35.8$, (b) 62.8, (c) 94.5, (d) 171.5.
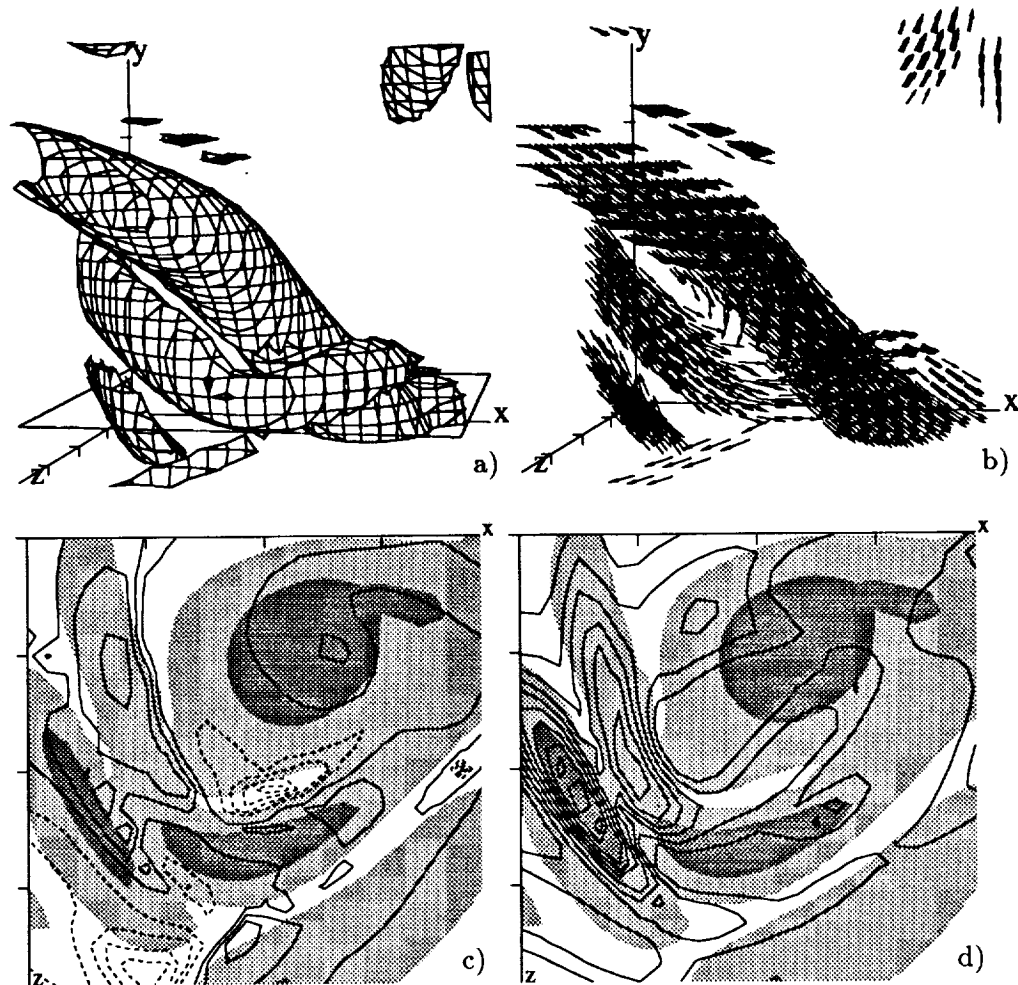
FIGURE 13. Portrait of a worm interaction, identified by a local maximum of the stretching term σ. $Re_\lambda = 94.5$. Length of axes, approximately 40η. (a) Intense vorticity isosurfaces, $|\omega| = 2.8\omega'$. (b) Vorticity vectors within the surfaces in (a). Vector lengths are proportional to vorticity. (c) Stretching and vorticity magnitude in the horizontal plane outlined in (a). Isolines are σ at $0.2\omega'$ increments; negative contours, dashed; zero contour not shown. Light gray, $\omega' < |\omega| < 2.8\omega'$. Dark grey, $|\omega| > 2.8\omega'$. (d) Same as (c), but isolines are strain magnitude $|s| > \omega'$ at $0.2\omega'$ intervals.

model is consistent with that of an axially stretched equilibrium Burgers' vortex. The distributions of radii and circulation along the length of a few typical worms is given in figure 12 for the four different Reynolds numbers. It is difficult to extract general trends from this figure and the number of actual coherent worms in each field is not enough to allow for rigorous statistics, but the most striking feature in these traces is the increase in complication as the Reynolds number increases.

Since we know from the previous analysis that an increase in Re_λ implies an increase in the Reynolds number of the vortices themselves, this is not surprising. It just means that, as their Reynolds number increases, the worms themselves are becoming turbulent, and it is an interesting question whether at high enough Re_λ they would retain enough coherence to be identified as separate objects. This question can not be answered directly here, but some analysis is possible on the type of complexity which is being added by increasing the Reynolds number. It is clear from figure 12 that the circulation traces are noisier that those of the radii. Part of the noise is doubtlessly due to detection problems, but the difference between the two sets of measurements is probably true. Since the circulation of a coherent vortex, defined as a fixed set of vortex lines, is constant along its length, the peaks in the circulation traces can be interpreted as interactions with other vortices, and it is the number of interactions that appears to increase with Re_λ.

Interactions between adjacent worms are indeed common in the flow fields and can often be found by looking for "active" spots in which either the vorticity or the stretching are especially large (see figure 13). Interactions between strong vortices and weaker vorticity are still more common, and they do not usually result in the destruction of the stronger partner.

The question of what is the origin of the stretching that generates the worms has still not been addressed. Figures 14 and 15 show two dimensional joint probability density functions for vorticity magnitude and strain. Figure 14a compares total strain $|s| = (S_{ij}S_{ij})^{1/2}$ with vorticity magnitude. It is clear from the figure that there is a correlation between these quantities, even if a rather weak one. Strong vorticity coexists with strong strain either because strong vortices generate high strains or because they are generated by them. That alternative is addressed in figure 14b, which compares vorticity magnitude with the stretching term σ. This histogram shows that the highest stretching rates are not associated with regions of high enstrophy, but with the background vorticity $O(\omega')$. In fact, the stretching associated with the highest enstrophy regions is fairly low and seems to scale well with ω', with little evidence of self stretching by the strongest structures. This apparent lack of correspondence between the behavior of the total strain and of the stretching component is also clear in figure 15, which compares both quanti-ties. Although there is clearly a correspondence between strong strain and large stretching in the sense that strong stretching or compression is associated more often with strong strains than with weak ones, the correspondence is only moder-ate, and the distribution of the ratio $\sigma/|s|$ is broad, peaking at low values rather than near the extremes. This ratio can be shown to be kinematically limited to the interval $\pm(2/3)^{1/2}$, which accounts for the sharp lateral cutoffs in the histograms in figure 15, but, within those limits, σ and $|s|$ are only weakly correlated. Strong strain does not necessarily mean strong compression or stretching, and the direction of the principal axis of the strain tensor seems to be relatively independent of the local vorticity direction. This is also seen in figures 13c-d, in which the total strain and the stretching terms are plotted independently. The total strain (fig. 13d) is relatively well correlated with the presence of strong vorticity, but the stretching
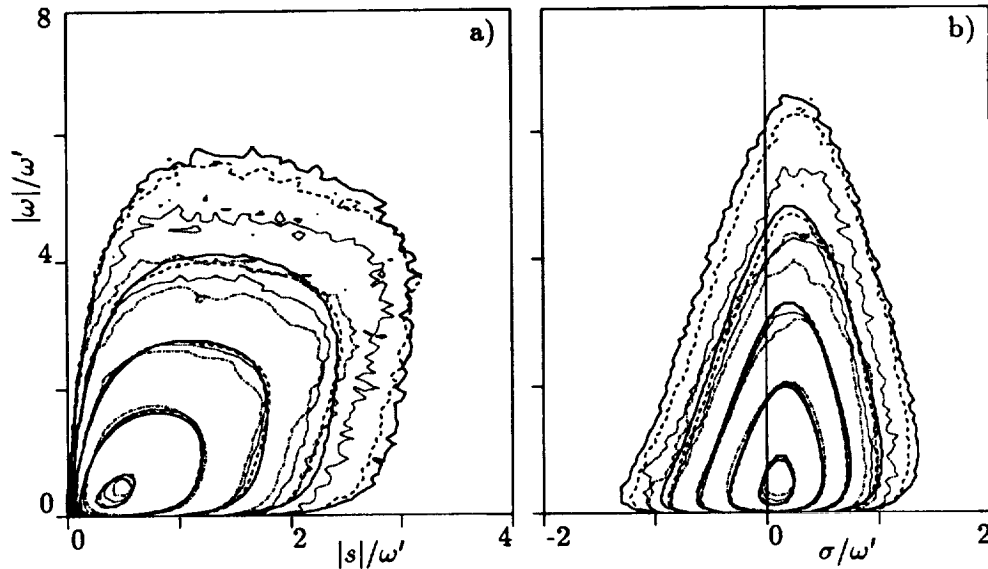
FIGURE 14. Joint probability density functions of strain magnitude and stretching versus vorticity magnitude. All values are normalized with ω'. Density contours are logarithmic and spaced by a factor of 10. Lines as in table 1.
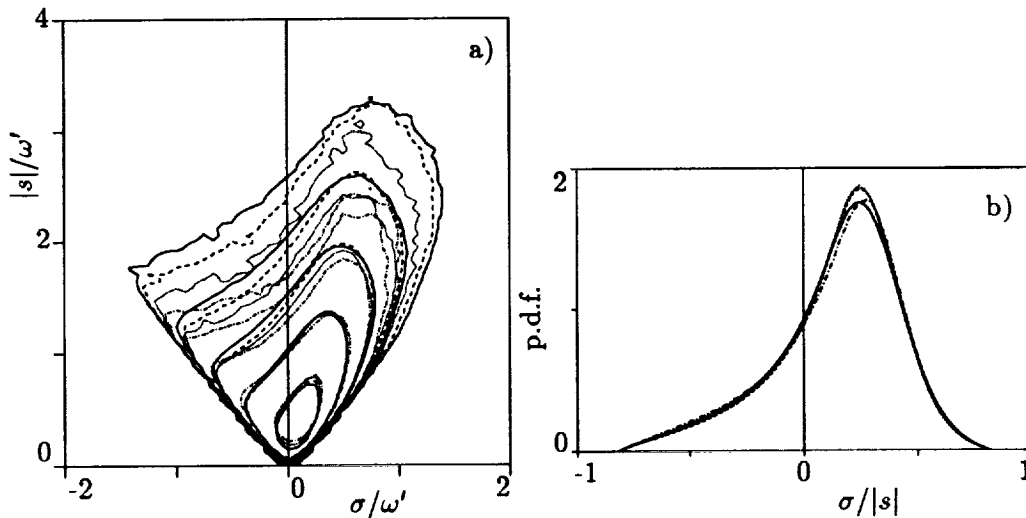

FIGURE 15. (a) Joint probability density functions of stretching versus strain magnitude. (b) Univariate probability density function of $\sigma/|s|$.

is much more randomly distributed, and both strong compressions and extensions are present close to each other. Plots of σ over larger sections of the flow field reveal a spotty distribution with a tendency to concentrate on the periphery of background (or intense) vorticity but not on its interior. Apparently, once vorticity gets stretched to a high enough amplitude, it decouples from the original strain field

and loses its orientation relative to it.

All this is consistent with the result obtained by previous investigators that there is little preferential alignment of the vorticity with the strongest strain axis at low vorticity magnitudes and that the alignment is to the intermediate (weakest) strain eigenvector in the intense regions (Ashurt *et al.*, 1987).

It is interesting to note that there seems to be a fairly good collapse of the distribution of $\sigma/|s|$ for different Re_λ and that this distribution is tilted both in figures 15 and 14b towards positive values of σ. This asymmetry corresponds to the negative skewness of the velocity derivatives in the flow field and is what makes possible the net amplification of vorticity.

One of the most striking features of these probability distributions is the similarity of their shape at different levels. The probability distributions, scaled on ω', collapse closely near the origin, corresponding to the good collapse of the one dimensional histograms in that range. Even away from that point where the higher Reynolds number cases display much stronger tails, the *shape* of the distributions are very similar for the high and for the low Reynolds flows. The outer, low probability isolines of the low Reynolds number distributions coincide almost exactly with the inner, high probability ones at high Re_λ. This suggest again that, whatever mechanism is responsible for the generation of high enstrophy or of high strain regions, it is independent of Reynolds number and that the only difference is that it becomes more common as the Reynolds number increases. The correspondence of inner and outer contours also suggests that the dynamics of the intense regions is not fundamentally different from that of the $O(\omega')$ background.

6. Discussion and conclusions

We have presented results on the structure of the intense vorticity regions in numerical turbulent flow fields at four different Reynolds numbers ranging from $Re_\lambda = 36$ to 171. Numerical resolution in terms of η and running time in large eddy turnover units were kept as constant as possible. The fields themselves are in statistical equilibrium with a suitable forcing, and the two higher Reynolds numbers are already in the "asymptotic" range in which dissipation becomes independent of Re_λ. In this sense, we are dealing with true turbulent flows. These last two fields also exhibit an inertial $k^{-5/3}$ spectral range that, in the highest Reynolds number case, spans almost a decade. The collapse of all the spectra in the dissipation range when expressed in Kolmogorov units is excellent, although there is a suggestion of a weak trend to slightly fuller spectra at higher Reynolds numbers (Fig. 1). The energy spectra in this range are exponential with an algebraic prefactor.

We give univariate histograms for several quantities related to the velocity gradients, especially for those related to the terms of the vorticity production equation. They are not gaussian, and they do not collapse in Kolmogorov units (ω'). There is a strong trend to longer tails of intense events at higher Reynolds numbers, which show no signs of converging to an asymptotic distribution within our experimental range.

We have confirmed in accordance with previous investigators that the physical

structure of these intense events is that of long coherent vortices of more or less elliptical cross section ("worms"). Although we lack adequate statistical confirmation, the eccentricity of the cross section appears to decrease as the Reynolds number increases. We have offered an explanation in terms of the relative strength of the strain and vorticity in those regions.

By means of an automatic tracking algorithm, we have computed the scaling laws for the kinematic properties of the worms. Their radii scale with the Kolmogorov microscale and their lengths with the integral scale of the flow, and their circulations increase with the Reynolds number as $Re_\gamma = \gamma/\nu \sim Re_\lambda^{1/2}$. With respect to this latter scaling, the data might be consistent with a slightly higher or lower exponent, but they are not consistent with the obvious guess that Re_γ should remain constant.

We have tried to clarify the dynamics of worm formation by means of joint probability densities of strain and vorticity. As expected, high enstrophy and high strain are associated with one another, although rather loosely, but, surprisingly, strong vorticity is not associated with high values of the stretching term, $\sigma = \omega S \omega / |\omega|^2$. In fact, the stretching of the high intensity worms is low and seems to scale well with the background vorticity ω'. Since the Burgers' length for a strain ω' is $(\nu/\omega')^{1/2} = \eta$, this is consistent with the scaling of the radius quoted above but strongly suggests that self stretching is not an important factor in the evolution of the intense vorticity.

An interesting observation is that the *shapes* of the probability isolines in the tails of the joint distributions are essentially similar to those in their central parts and that they are quite independent of the Reynolds number. This, together with the previous observation on the lack of self stretching, suggests that the worms are only particularly intense realizations of the background vorticity field, $|\omega| > \omega'$. This background component is responsible for most of the turbulent dissipation (80%) but fills a much smaller percentage of the volume (25%). We have presented some indications that it is concentrated in large scale, turbulent, vortex sheets separating the energy containing eddies at the integral scales. The worms are imbedded within this background (Figs. 6-7).

We have also shown by removing the worms artificially from an equilibrium turbulent field and studying its further development that worms are not especially important in the overall dynamics of turbulence and that they are only responsible for a fraction of the kinetic energy proportional to the volume that they occupy and for a fraction of the dissipation proportional to their integrated enstrophy. Both are small numbers at the Reynolds numbers of our simulations but could become bigger in the limit $Re_\lambda \gg 1$. We have also shown that worms are not artifacts of forced turbulence. If they are removed from a decaying field, they reappear within a small fraction of a turnover time.

The lack of convergence of the probability distributions appears to support the multifractal models of turbulence in which cascades of increasing intensities are concentrated on increasingly small regions of space. The way in which this local concentration is implemented is, however, somewhat surprising, although consistent with previous indications from the near wall region of turbulent channels. Instead

of having vortices of fixed circulation being stretched more at higher Reynolds numbers, our data imply increasingly stronger vortices being stretched by a fixed amount.

The question of how these vortices are formed will not be addressed here and will be the subject of coming publications. The purpose of this paper is to present a data base that can be used to constrain any such future model. It may still be of some interest to discuss briefly the nature of some of these constraints. There are three basic problems: how the large vorticities are generated, why Re_γ increases with Re_λ, and how a small scale structure can maintain a length of the order of the macroscale.

The first question presents no qualitative difficulty, although its quantitative answer lies at the heart of turbulence theory. High vorticity is generated by stretching, and stretching is generated by the integrated effect of the rest of the vorticity in the flow. We have seen that the highest vorticity has transverse dimensions of the order of η. This is already implicit in Kolmogorov theory and implies that the prevailing rate of strain is $O(\omega')$. Since we know from the histograms in figure 3 that the predominant vorticity is also $O(\omega')$, this implies that the Reynolds number of a typical dissipative eddy, Re_γ, is $O(1)$ and independent of Re_λ. This is in agreement with intuitive stability arguments.

A relatively small percentage of dissipative eddies (at our Re_λ) seems to be strained while maintaining a much larger Re_γ. Large Reynolds number vortex sheets are subject to inviscid instabilities and will quickly roll into individual vortices, but columnar vortices are linearly stable, although they are subject to inertial waves and will probably break up if perturbed hard enough. There is little doubt that a sufficiently high Reynolds number vortex will eventually become internally turbulent, but it may survive long enough to be observed in rare situations. We have seen in figure 12 that worms become "noisier" as Re_λ increases, in general agreement with this argument. Note also that the evidence suggests that the strong vortices are subject to rates of strain that are much weaker than their own vorticity. Under those circumstances, they would behave as essentially unstrained and they could only be appreciably perturbed by self, or mutual, interaction.

It might even be possible to shed some light on the scaling law $Re_\gamma \sim Re_\lambda^{1/2}$. The relation that comes to mind is

$$u'\eta/\nu \sim Re_\lambda^{1/2},$$

which implies that the velocity increment across an intense worm is of the same order as the characteristic velocity of the energy containing eddies. A simple model is that of large eddies straining vorticity at the interfaces in which they meet (see figures 6 and 7). On most occasions, the vortex sheets generated in that way become unstable and break into smaller eddies that strain each other into the $O(\omega')$ vorticity background. Occasionally, however, a small part of the vortex sheet survives the instability and is strained to thickness η while still retaining across itself the full velocity difference u'. The eventual roll-up of this sheet generates worms.

Note that this model does not predict the conditions for the formation of worms, but that it singles out the observed scaling law as an upper limit for Re_γ, since

strong intermittency of the velocity itself is not observed. Note also that it suggests that the initial stretching takes the form of sheets since the velocity increment across a stretched sheet is maintained while that of a cylindrical vortex increases in inverse proportion to its diameter.

Finally, the problem of the long lengths of the worms is harder. It is inconceivable that a rate of strain $O(\omega')$ remains coherent over a region of space of size $O(L)$. Since we know that velocities are only $O(u')$, the largest possible coherence length for a strain ω' is $u'/\omega' \sim \lambda$. This suggests that worms are not formed in a single stage, but that they grow or coalesce along their lifetimes. Several possible mechanisms come to mind, but they are beyond the scope of this paper.

Acknowledgements

REFERENCES

ASHURST, W. T., KERSTEIN, A. R., KERR, R. M. & GIBSON, C. H. 1987 Alignment of vorticity and scalar gradient with strain in simulated Navier Stokes turbulence. *Phys. Fluids.* **30**, 3243-3253.

BATCHELOR, G. K. 1953 *The theory of homogeneous turbulence.* Cambridge Univ. Press.

BATCHELOR G. K. & TOWNSEND, A. A. 1949 The nature of turbulent motion at large wave numbers. *Proc. Roy. Soc. London.* **A 199**, 238-255.

BETCHOV, R. 1956 An inequality concerning the production of vorticity in isotropic turbulence. *J. Fluid Mech.* **1**, 497-504.

CANUTO, C., HUSSAINI, M. Y., QUARTERONI, A. & ZANG, T. A. 1987 *Spectral methods in fluid dynamics.* Springer, pp. 85-86.

DOUADY, S., COUDER, Y. & BRACHET, M. E. 1991 Direct observation of the intermittency of intense vorticity filaments in turbulence. *Phys. Rev. Lett..* **67**, 983-986.

HOSOKAWA, I. & YAMAMOTO, K. 1990 Intermittency of dissipation in directly simulated fully developed turbulence. *J. Phys. Soc. Japan.* **59**, 401-404.

JIMÉNEZ, J. 1991 On small scale vortices in turbulent flows. *CTR Annual Res. Briefs.* , 45-56 (see also *Phys. Fluids*, **A 4**, 652-654).

KERR, R. M. 1985 Higher order derivative correlation and the alignment of small-scale structures in isotropic numerical turbulence. *J. Fluid Mech.* **153**, 31-58.

KOLMOGOROV, A. N. 1941 The local structure of turbulence in incompressible viscous fluids a very large Reynolds numbers. *Dokl. Nauk. SSSR..* **30**, 301-305 (see e.g. L.D. Landau & E.M. Lifshitz, 1959, *Fluid mechanics*, Pergamon, pp. 116-123).

RUETSCH, G. R. & MAXEY, M. R. 1991 Small scale features of vorticity and passive scalar fields in homogeneous isotropic turbulence. *Phys. Fluids.* **A 3**, 1587-1597.

SHE, Z-S., JACKSON, E. & ORSZAG, S. A. 1990 Intermittent vortex structures in homogeneous isotropic turbulence. *Nature.* **344**, 226-228.

SIGGIA, E. D. 1981 Numerical study of small scale intermittency in three dimensional turbulence. *J. Fluid Mech.* **107**, 375-406.

SREENIVASAN, K. R. 1984 On the scaling of the turbulence energy dissipation rate. *Phys. Fluids.* **27**, 1048-1051.

TOWNSEND, A. A. 1951 On the fine scale structure of turbulence. *Proc. Roy. Soc. London.* **A 208**, 534-542.

VAN ATTA, C. W. & ANTONIA, R. A. 1980 Reynolds number dependence of skewness and flatness factors of turbulent velocity derivatives. *Phys. Fluids.* **23**, 252-257.

VINCENT, A. & MENEGUZZI, M. 1991 The spatial structure and statistical properties of homogeneous turbulence. *J. Fluid Mech.* **225**, 1-25.

WEI, T. & WILLMARTH, W. W. 1989 Reynolds-number effects on the structure of a turbulent channel flow. *J. Fluid Mech.* **204**, 57-95.

Appendix I: Data processing for vortex radii and circulations.

In order to elucidate the geometric structure of the worms, an algorithmic definition is needed for the set of points in space which will be taken to constitute a single worm. Such definitions necessarily contain some degree of arbitrariness, and the one used here is certainly no more than one among many possibilities.

We are interested in the strong vortical regions, and we take maxima of enstrophy as starting points. We define a worm axis and core starting with:

(1) Find the point of maximum enstrophy not yet included in any worm core. This is the first worm-axis point of a new worm.

From that point one could reasonably proceed along the vortex line through the point to define a worm centerline. However, an elongated region of high enstrophy, which we take intuitively as a worm, does not have vorticity perfectly aligned along its axis, nor does a given vortex line necessarily remain within it over its entire length. Therefore, to increase the chances of staying within the high-vorticity structure, the worm-core definition is taken as:

(2) Follow the local vorticity vector from the current worm-axis point until it intersects the next grid plane, then choose as worm-core points the four grid points in this plane which surround the point of intersection. The new worm-axis point is the one with the maximum enstrophy.

This is done in both directions from the first worm-axis point until:

(3) The worm is taken to end when the new maximum enstrophy is below the global mean value, ω'^2, or when the worm axis intersects its own or another worm's core.

From the set of worm-axis points we compile radial distributions of axial vorticity in the next two steps:

(4) Define the radial plane around a given worm-axis point as that set of points for which the given axis point is the closest point on the worm axis.

(5) Average the component of vorticity parallel to the worm axis (at the given axis point) over these radial-plane points. The averaging is done into radial bins of width Δx.

With the distributions of axial vorticity as a function of distance from and position along the axis, we can compute approximations to the worm radius and circulation as functions of axial position. The radial distribution is fitted to a gaussian shape, with the measured value of ω_0 the axial vorticity at the axis. The $1/e$ radius, R, of the distribution is estimated from the distance r_q at which the vorticity falls to a fraction q of its value at the axis:

$$R = r_q/(-\ln(q))^{\frac{1}{2}}.$$

This estimation is repeated for several $q \in (0.25 - 0.75)$, and the average of the different estimations is taken as the final radius. The circulation γ at this section is then approximated by integrating the gaussian, assuming axisymmetry:

$$\gamma = \omega_0 \pi R^2$$

We have found this procedure to give clearer results than computing the circulation directly from the radial distribution. The latter is hampered by the difficulty of doing the circulation integral over a quite noisy distribution containing vorticity from other worms and the background.

Steps (1)-(5) are repeated to obtain a database containing a few tens of worms. Statistics of radius and circulation are collected over this database.